



EFFECT OF PRESTRESS LOSS ON SEISMIC VULNERABILITY OF POST-TENSIONED PRECAST CONCRETE SEGMENTAL BRIDGE

Terry Y.P. Yuen⁽¹⁾, Wang-wen Chan⁽²⁾, Xiangming Zhou⁽³⁾, Trissa Deb⁽⁴⁾, Yang Liu⁽⁵⁾, Hanhui Zhang⁽⁶⁾

⁽¹⁾ Assistant Professor, National Chiao Tung University, Taiwan, R.O.C., terryyyp@nctu.edu.tw

⁽²⁾ Structural Engineer, CECI Engineering Consultants, Inc., Taiwan, R.O.C., a8012182012@gmail.com

⁽³⁾ Professor, Brunel University London, United Kingdom, xiangming.zhou@brunel.ac.uk

⁽⁴⁾ PhD Candidate, National Chiao Tung University, Taiwan, R.O.C., trishadeb23@gmail.com

⁽⁵⁾ Associate Professor, College of Civil Engineering, Huaqiao University, China, yliubp@hqu.edu.cn

⁽⁶⁾ Structural Engineer, Ove Arup and Partners Hong Kong Ltd., Hong Kong, China, ethanzhh@gmail.com

Abstract

Being cost-effective, rapid construction, high transportability, and maintainability, post-tensioned precast concrete segmental bridges (PT-PCSBs) have been one of the most preferred choices for long-span bridges located on sites that are restrictive to access. Typical bridge superstructures are designed to behave elastically or capacity-protected under earthquakes. Yet, deterioration of aging bridges due to steel corrosion and spalling of concrete can cause additional steel relaxation and deflection, resulting in prestress loss and degraded structural performances at different limit states. Furthermore, significant loss of prestress may lead to premature decompression and therefore increase seismic vulnerability. In this regard, this paper numerically investigates the effects of prestress loss on seismic performances and fragility of PT-PCSBs at different limit states. The prototype is a 44.25 m long, 2.4 m depth and 10.2 m wide highway bridge with 14 precast reinforced concrete box-girder segments. The segmental bridge was post-tensioned by 12 unbonded external tendons which form an approximate parabolic profile to provide the flexural resistances.

Rigorous and detailed 3D discrete finite element (DFE) models were developed for Incremental Dynamic Analysis (IDA) with 10 bi-directional earthquake ground motions (GMs). The transverse direction of the PT-PCSBs is subject to the stronger component of the GMs, while the longitudinal direction is subject to the weaker component. Each concrete bridge segment is modeled by continuum finite element mesh equipped with damage-plasticity constitutive law. The normal and tangential interactions between two adjacent concrete segment surfaces are enforced based on the contact mechanics. The tendons anchor behavior is simulated by multiple coupling constraints and the translational connectors are used to simulate the expected tendon slip behavior from the deviators.

The fragility functions of the maximum transverse, longitudinal, and vertical deflection ratios against the corresponding spectral accelerations at the first mode are constructed using the IDA curves corresponding to the 10 GMs. Based on the analysis results, it was found that 20% prestress loss can lead to 10% to as much as 14% reduction in the structural load-carrying capacity and 5% increase in the collapse probability. The prestress loss has limited effects on the exceedance probability of smaller deflection ratios in the transverse and vertical directions but significantly affected the vertical responses under the earthquake excitations with low intensities. The strong coupling of the vertical-longitudinal vibration modes results in significant vertical deflection responses even though the input excitations do not contain any vertical component.

Keywords: precast segmental bridges; prestress loss; discrete finite element; IDA; unbonded external tendons



1. Introduction

Being cost-effective, rapid construction, high transportability, reduction of environmental impacts, and maintainability, post-tensioned precast concrete segmental bridges (PT-PCSBs) have been one of the most preferred choices. The precast bridge segments are often connected by post-tensioned tendons and shear key joints which respectively provide the flexural resistance and shear resistance. Ducts can be installed inside the bridge segments for holding and positioning the prestressing tendons. In bonded PT-PCSBs, the ducts are grouted to protect and bond the internal tendons to the segments. The flexural behaviour of bonded PT systems is similar to pre-tensioned systems and can be analysed by elementary beam theory. The behaviour of PT-PCSBs with unbonded tendons, which can be placed internally or externally, is far more complicated since the tendon forces are discontinuously transferred to the concrete only at the anchorages and deviators which connect the tendons and the segments. When unbonded PT-PCSBs subject to bending, plane sections no longer remain due to the tendon slip and thus the elementary beam theory may not be able to accurately analyse the flexural behaviour [3]. The complicated stress distributions also make the prediction of the prestress losses becomes a difficult task.

Despite the uncertain and complicated behaviour, the popularity of unbonded PT-PCSBs has been increasing over the past decade due to the easier and safer demolition by releasing the prestressing forces in the unbonded tendons [1]. The external tendons also allow quick inspection of the tendon condition and easier maintenance compared to internal tendons. Furthermore, it has been shown that prestressed structures/members with unbonded tendons could have better seismic performances. For instances, Ou *et al.* [2] experimentally investigated the seismic behaviour of precast segmental unbonded post-tensioned concrete bridge columns for use in high seismic regions. Four large-scale specimens were designed and tested with lateral cyclic loading and it demonstrated excellent drift capacities. Typical seismic design of bridges requires the superstructures to be capacity protected and behave elastically or undergo very limited inelastic deformation under seismic loading. Bu *et al.* [5] demonstrated experimentally that the unbonded post-tensioned bridge columns with energy dissipation bars showed higher lateral strength and lower residual drift. The bonded counterpart with an appropriate bar arrangement also showed higher lateral strength but experienced large post-tensioned stress loss.

If the maintenance and protection are not carried out properly for unbonded PT-PCSBs, corrosion of the tendons and concrete flaking and spalling [4] can occur that lead to degraded strength and stiffness. The softened bridge structures may undergo additional deformation that results in additional loss of the prestress force in the tendons. Contrasting to prestressed structures with bonded tendons, the prestress loss has direct effects on the structural performances of prestressed structures with unbonded tendons. The excessive loss of prestress not only can significantly affect the structural load-carrying capacity of the PT-PCSBs with unbonded tendons [3] but also lead to premature decompression after which the bending stiffness will drop significantly and may subsequently increase the structural vulnerability. Moreover, excessive deflections can damage the non-structural components on the bridge superstructures which can inflict significant repair cost and should be prevented at frequent earthquake ground motions with low intensities.

Therefore, the effects of prestress loss on the seismic performances and fragility of PT-PCSBs with unbonded external tendons require more thorough exploration. A rigorous parametric study with detailed and experimentally validated numerical models has been an effective tool to investigate the nonlinear structural responses [5,6]. In this paper, a rigorous and detailed 3D discrete finite element model (DFEM) has been developed for a prototype PT-PCSB with unbonded external tendons. The DFEM can simulate not only the global load-deflection behaviour but also the detailed frictional interaction between the contacting surfaces of bridge segments, local joint openings, strain/stress changes in the tendons, and slips of the tendons from the ducts. Incremental Dynamic Analyses are then performed with 10 earthquake ground motions for a PT-PCSB model with the original prestress P_e and a model with 20% prestress loss i.e. $0.8P_e$. The fragility functions are then constructed based on the 10 IDA curves for each model. The effects of prestress loss on the failure mechanisms, collapse probability, structural capacity, and exceedance probabilities of different deflection limit states are studied based on the analysis results.



2. Prototype and Modelling

2.1 Prototype

A highway bridge span, as part of the Second Stage Expressway System (SES), in Bangkok was adopted as the prototype PT-PCSB for the numerical investigation in this study. The span, supported on 4 elastomeric bearings at the two ends, was 44.25 m long, 2.4 m depth and 10.2 m wide with 14 precast reinforced concrete box-girder segments. The structural design of the bridge adopted the AASHTO specifications [8]. The post-tensioning of the bridge was carried out with 12 unbonded external tendons, of which 10 longer tendons formed from 19K15 strands ($A_{ps} = 2850 \text{ mm}^2$) were anchored at the two ends and 2 shorter tendons formed from 12K15 strands ($A_{ps} = 1800 \text{ mm}^2$) were anchored at the bottom of the 4th and the 11th segments. The 10 longer tendons (T1-5L & T1-5R) were anchored at the two ends of the span and were held down by the deviators in the 4th, the 7th, and the 11th segments, while the 2 shorter tendons (T6L & T6R) were also held down by the deviator at the 7th segment to produce an approximate parabolic profile with the lowest point at the 7th segment. The tendons were protected by cement-grouted high-density polyethylene ducts (HDPE). The segments were also interlocked by dry key joints which transfer shear force between shear segments. Each segment was also internally reinforced with non-prestressing 24-mm diameter steel rebar spaced at 100 mm in both longitudinal and transverse directions. The cross-section and tendon profiles of the bridge segments are shown in Fig 1(a). Further details of the SES highway bridge span can be found in Takebayashi et al. [7]. The material properties of the prototype are summarised in Table 1. The back-calculated effective prestress force was 38433 kN just before the test [7], which produced an average prestress of $p_{ei} = 0.62 f_{pu} = 1198 \text{ MPa}$ in the tendons. Weights in form of the steel billets were gradually placed on segments 4-6 and 9-11 until the bridge collapsed. The failure load was 909.14 tons, which was corresponding to a mid-span moment of 58.2 MN·m. Another important load stage was the observed decompressed load of 562.1 tons (36.5 MN·m) after which the segmental bridge stiffness decreased rapidly.

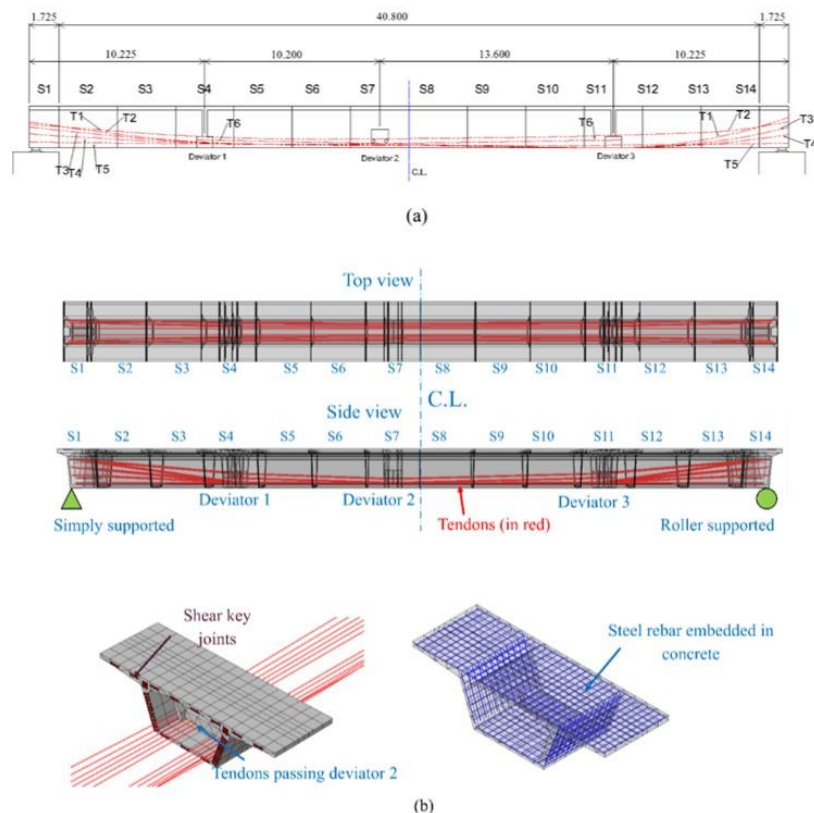


Fig. 1 – Unbonded PT-PCSB [7]: (a) side view; (b) model (all dimensions in m).



Table 1 – Material properties of the bridge prototype [7].

Material	Modulus of elasticity (GPa)	Strength (MPa)
Concrete	43	55-62 (compressive strength f_{cc})
Non-prestressing steel	210	390 (yield strength f_{sy})
Tendons	193	1920 (breaking strength f_{pu})

2.2 Model development

A highly detailed three-dimensional finite element model for the prototype unbonded PT-PCSB was developed with ABAQUS [9] to simulate the destructive loading test by Takebayashi *et al.* [7]. Overview of the model and the finite mesh is shown in Fig 1(b). The bridge span is simply-supported at the two bottom corners of segment 1 and roller-supported at two bottom corners of segment 14. Each bridge segment is modelled with continuum linear 3D stress elements (C3D8R) and the original geometry is reproduced in the model. The internal steel reinforcement (non-prestressing) in each segment is modelled with linear 3D truss elements (T3D2), which are bonded to the surrounding concrete using the embedded region constraint. The dry-joint shear keys as shown in Fig 1(b), which provide interlock and shear stress transfer for two adjacent bridge segments, are modelled with C3D8R elements. The shear keys have one face tied to the surface of one segment and the body embedded in the adjacent segment.

Besides the shear keys, contact interaction is enforced for the contacting surfaces of the bridge segments. The friction coefficient is assumed as 0.6 following the recommendation by EC2 [10] and a normal contact stiffness $S_n = 520$ kN/mm is specified to prevent penetration of the contacting surfaces. The contact interaction can model the compressive force transfer and friction of the contacting surfaces. Such modelling method combining contact interaction and deformable element analysis is known as discrete finite element modelling (DFEM) [6] which can effectively simulate the joint/crack opening and closing behaviour. The interactions and constraints applied in the model are summarized in Table 2. The external tendons are modelled with linear beam elements (B31). The anchored ends of the tendons are constrained to the corresponding segment surface using the kinematic coupling. The interaction between the deviators and the tendons is modelled with translators which allows the tendons to move along the bridge longitudinal direction with a restoring stiffness $k_l = 0.95$ kN/mm, while the other degree of freedoms is restrained.

Table 2 – Constraints and interactions of the components

Component (s)	Constraint/interaction	Modelling parameter(s)
Non-prestressing rebar	Embedded in concrete segments	-
Shear keys	One face tied on a segment surface and the body embedded in the adjacent segment	-
Segment-segment interfaces	Contact interaction	$S_n = 520$ kN/mm (normal stiffness) $\mu = 0.6$ (friction coefficient)
Tendon-deviators	Translators – movement in the longitudinal direction only	$k_l = 0.95$ kN/mm (translational stiffness)
Tendon anchorage	Kinematic coupling to the concrete segment surfaces	-



2.3 Constitutive models of the materials

The multi-axial elastoplastic behaviour of concrete is modelled with the non-associate Barcelona model [11], of which yield surface and the hyperbolic Drucker-Prager flow potential. The uniaxial inelastic compressive stress-strain curve $\sigma_c(\varepsilon)$ for $\varepsilon \geq 0$ adopted to define the evolution of the yield surface follow the Kratzig and Polling (2004) model [12],

$$\sigma_c(\varepsilon) = \frac{E_{ci} \frac{\varepsilon}{f_{cc}} + \left(\frac{\varepsilon}{\varepsilon_{cc}}\right)^2}{1 - \frac{\varepsilon}{\varepsilon_{cc}} \left(E_{ci} \frac{\varepsilon}{f_{cc}} - 2\right)} f_{cc} \quad (\text{ascending } \varepsilon < \varepsilon_{cc}) \quad (1)$$

$$\sigma_c(\varepsilon) = \left(\frac{2 + \gamma_c f_{cc} \varepsilon_{cc}}{2 f_{cc}} + \gamma_c \varepsilon + \frac{\gamma_c}{2 \varepsilon_{cc}} \varepsilon^2\right)^{-1} \quad (\text{descending } \varepsilon \geq \varepsilon_{cc}) \quad (2)$$

where E_{ci} , f_{cc} , and ε_{cc} are the tangent modulus of elasticity, the peak uniaxial compressive strength, and the accompanying strain at f_{cc} respectively. γ_c is a parameter controlling the area under the tensile stress-strain curve. On the other hand, the uniaxial inelastic tensile stress-strain curve $\sigma_t(\varepsilon)$ for $\varepsilon < 0$ is based on the CEB-FIP (2010) model [13]:

$$\sigma_t(\varepsilon) = E_{ci} \varepsilon \quad (\sigma_t \leq 0.9 f_{ctm}) \quad (3)$$

$$\sigma_c(\varepsilon) = f_{ctm} \left(1 - 0.1 \frac{0.00015 - \varepsilon}{0.00015 - 0.9 f_{ctm} / E_{ci}}\right) \quad (0.9 f_{ctm} < \sigma_t \leq f_{ctm}) \quad (4)$$

$$\sigma_c(\varepsilon) = f_{ctm} \left(1 - 0.8 \frac{\varepsilon}{\varepsilon_1}\right) \quad (\varepsilon \leq \varepsilon_1) \quad (5)$$

$$\sigma_c(\varepsilon) = f_{ctm} \left(0.25 - 0.05 \frac{\varepsilon}{\varepsilon_1}\right) \quad (\varepsilon_1 < \varepsilon \leq \varepsilon_c) \quad (6)$$

where f_{ctm} is the peak tensile strength, $\varepsilon_1 = G_t / f_{ctm} l_{eq}$, and $\varepsilon_c = 5 G_t / f_{ctm} l_{eq}$ in which G_t taken as 0.1423 N/mm^2 is the mode I fracture energy. l_{eq} is the element characteristic length taken as 600 mm in this study. The compressive and tensile stress-strain curves are shown in Figs. 2 (a) & (b) respectively.

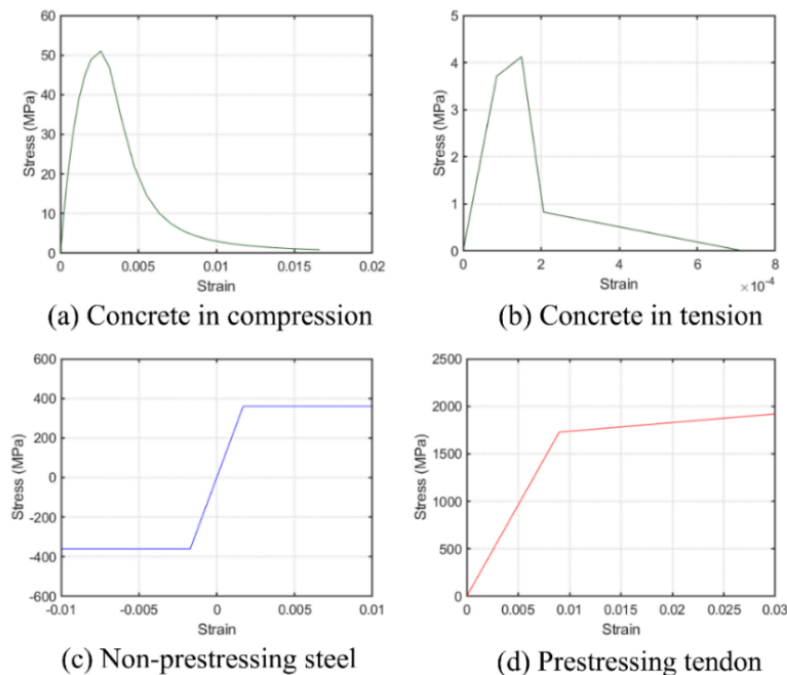


Fig. 2 – Stress-strain curves of concrete, steel rebar, and prestress tendon.



The stress-strain behaviour of the normal steel rebar is modelled with a linear perfect-plastic model with the yield strength $f_{sy} = 390$ MPa and modulus of elasticity $E_s = 210$ GPa. A bilinear stress-strain behaviour is assumed for the tendons with the breaking strength, $f_{pu} = 1920$ MPa and yield strength $f_{py} = 0.9f_{pu} = 1728$ MPa. The stress-strain curves of the non-prestressing steel and prestressing tendons adopted in this study are shown in Figs. 2 (c) & (d) respectively. The prestressing force $P_e = 38433$ kN is introduced to the tendons by the thermal stress method

$$\Delta T = - \frac{P_e}{c \cdot E_{ps} \cdot A_{ps}} \quad (7)$$

where $c = 13 \text{ }^\circ\text{C}^{-1}$ is the coefficient of thermal expansion and ΔT is the induced temperature change.

3. Fragility Analysis

3.1 Selected ground motions and spectral accelerations

Bi-directional nonlinear time histories analysis (Bi-NTHA) was performed using the developed DFEM model to investigate the prestress loss effects on the seismic performances and fragility of the PT-PCSB. Ten earthquake ground motions (GMs) each with two horizontal components are selected to perform the analysis and their characteristics are summarised in Table 3. In the Bi-NTHA, the transverse (T) direction of the bridge is subject to the stronger horizontal component of the GM, while the longitudinal (L) direction is subject to the weaker component. The range of the 30-m shear-wave velocities V_{30} of the sites is between 198 m/s – 496.2 m/s, which falls within the soil profile type C and the lower bound of type B according to Eurocode 8 [14]. The significant duration is defined based on the 5-95% of the normalized Arias intensity [15]. Five of the GMs are near field with the Joyner-Boore distances $R_{jb} < 15$ km and the others are far-field with $R_{jb} > 20$ km.

Table 3 – Characteristics of the selected ground motions and spectral accelerations

GM Label	Station, earthquake, M_w	V_{30} (m/s)	R_{jb} (km)	Significant duration (s)	Direction	Original PGA (g)	PGAh (g)	$S_{a1}/PGAh$
HSP-T	Hollister South & Pine, 1989 Loma Prieta, 6.9	282.1	27.67	24.7	000°	0.3698	0.3731	2.606
HSP-L					090°	0.1786		0.371
CLDD-T	Coyote Lake Dam Downstream, 1989 Loma Prieta, 6.9	295.0	20.44	13.1	285°	0.1793	0.1863	1.057
CLDD-L					195°	0.1596		0.847
ASH-T	Agnews State Hospital, 1989 Loma Prieta, 6.9	239.7	24.27	29.7	000°	0.1695	0.1852	0.920
ASH-L					090°	0.1609		0.954
SCA-T	Sunnyvale Colton Ave, 1989 Loma Prieta, 6.9	267.7	23.92	26.7	360°	0.2071	0.2191	1.304
SCA-L					270°	0.2070		1.058
WAHO-T	WAHO, 1989 Loma Prieta, 6.9	388.3	11.03	11.9	090°	0.6324	0.6458	0.849
WAHO-L					000°	0.3696		0.572
EL13-T	El Centro Array 13, 1979 Imperial valley, 6.5	249.9	21.98	23.4	230°	0.1384	0.1414	0.575
EL13-L					140°	0.1172		0.805
CHY80-T	CHY080, 1999 Chi-chi, 7.7	496.2	0.11	26.2	NS	0.8567	0.9217	2.677
CHY80-L					EW	0.8090		2.337
CHY06-T	CHY006, 1999 Chi-chi, 7.7	438.2	9.79	30.6	NS	0.3582	0.3850	2.332
CHY06-L					EW	0.3543		1.548
KOTA-T	Takatori, 1995 Kobe, 6.9	256.0	1.46	11.6	090°	0.6573	0.7563	1.655
KOTA-L					000°	0.6156		1.202
KOPO-T	Port IsInd, 1995 Kobe, 6.9	198.0	3.31	13.2	000°	0.3475	0.4342	1.626
KOPO-L					090°	0.2876		1.258

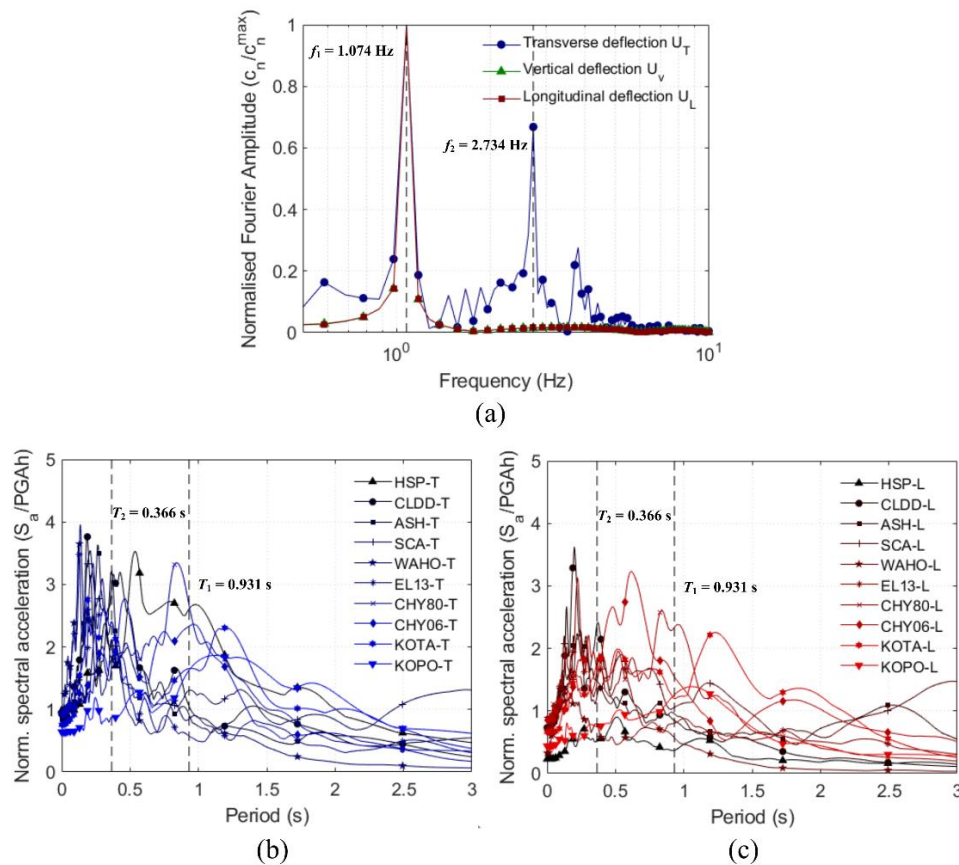


Fig. 3 – (a) Fourier spectra of the PT-PCSB responses under the white noise excitation; response spectra in the (b) transverse direction and (c) in the longitudinal direction (damping ratio = 5%).

Based on the Fourier spectra of the PT-PCSB responses under the white noise excitation (Fig 3 (a)), the fundamental vibrational frequency is $f_1 = 1.074$ Hz, which corresponds to the fundamental period $T_1 = 0.931$ s. The longitudinal and vertical vibrations are strongly coupled. The fundamental vibration mode is dominated by the vertical deflection coupled with the longitudinal and transverse deflections. The second vibrational frequency which is related to a pure transverse deflection mode is $f_2 = 2.734$ Hz ($T_2 = 0.366$ s). The elastic response spectra (damping ratio = 5%) of the selected GMs in the transverse and longitudinal directions are shown in Figs 3 (b) & (c) respectively. The spectral accelerations S_{a1} at the first mode are determined from the response spectra and the normalised values with respect to the horizontal peak ground acceleration (PGA_h) of each GM are summarised in Table 3.

3.2 Seismic responses and IDA curves

In this study, the motions of bearings and substructures are not considered and the PT-PCSB models are directly excited with the selected GMs at the supports. Hence, the excitations can be considered as the seismic waves transferred from the bearings. Incremental Dynamic Analysis (IDA) [16] was performed by repeating the Bi-NTHA with increasing PGA_h for each GM until the collapse of the PT-PCSB is observed. An IDA curve for a specific GM is then constructed by plotting the increasing spectral accelerations at the first mode S_{a1} against the maximum deflection ratios Δ/L obtained from the NTHA. Three group of IDA curves (Fig. 4) were constructed which are corresponding to the transverse (S_{a1}^T vs Δ^T/L), vertical (S_{a1}^L vs Δ^V/L), and longitudinal (S_{a1}^L vs Δ^L/L) directions respectively. Due to the strong coupling between the longitudinal and vertical vibrations (Fig. 3(a), the vertical deflection (Δ^V) is correlated with the longitudinal spectral acceleration S_{a1}^L in the construction of the vertical IDA curves.

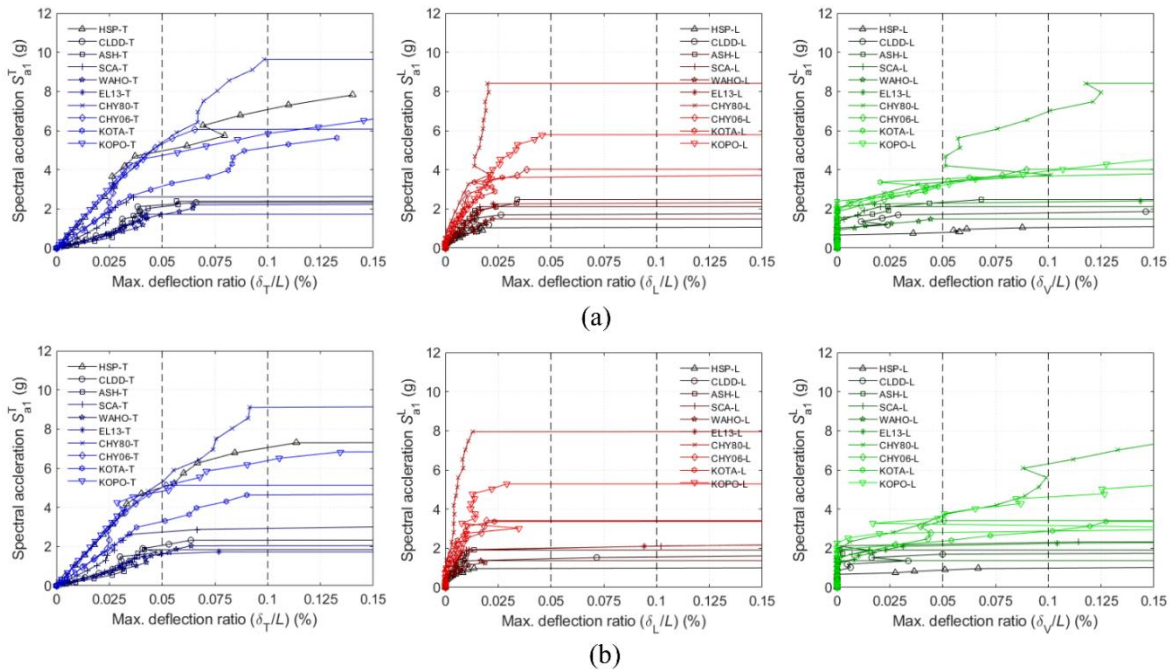


Fig. 4 – IDA curves: (a) PT-PCSB with $P_e = 38433$ kN (b) PT-PCSB with $0.8P_e = 30746$ kN. (note: the initial vertical and longitudinal deflection ratios of 0.09 % & 0.016% for P_e and 0.07% & 0.013% for $0.8 P_e$ due to prestress and gravity loads have been subtracted from the total deflection ratios).

At the ultimate failure stage, the concrete segments near the end segments developed severe damage and then the collapse of PT-PCSB occurred under the self-weight. Fig. 5. illustrates the damage evolution in the PT-PCSBs under the KOTA excitations at the intensities that the structural collapse occurs ($PGA_h = 2.4$ g with $S_{a1}^T = 3.97$ g & $S_{a1}^L = 2.88$ g for the model with $0.8P_e$ and $PGA_h = 2.8$ g with $S_{a1}^T = 4.63$ g & $S_{a1}^L = 3.37$ g for the model with P_e) and Fig. 6. shows the corresponding input acceleration and displacement response time histories. Besides the collapse state, two deflection limits $(\Delta/L)_{limit}^1 = 0.1\%$ & $(\Delta/L)_{limit}^2 = 0.05\%$ are considered. The first limit of 0.1% is the serviceability deflection limit specified by AASHTO [17] for bridges accessible for pedestrians. However, as shown in Fig. 4, significant transverse inelastic deformation or even collapse had occurred already before the deflection ratios reached 0.1%. and the “yielding” or the significant change of stiffness of the PT-PCSBs began around 0.05%.

3.3 Effects of prestress loss on the structural fragility

The probability or fragility functions of the spectral acceleration S_{a1} at the first mode for the three limit states: collapse state and deflection limit states of $(\Delta/L)_{limit}^1 = 0.1\%$ & $(\Delta/L)_{limit}^2 = 0.05\%$ are constructed from the n-IDA curves (Fig. 4), where n = 10 is the number of GMs. The spectral acceleration $\hat{S}_{a1,i}$ corresponding to a specific limit state is recorded from the i -th IDA curve and then statistical analysis is performed to construct the fragility functions with the collected $\hat{S}_{a1,i=1,2,\dots,10}$ from the 10 IDA curves. The fragility functions can be fitted by a log-normal distribution function [18] with the mean $\ln \theta$ and the standard deviation β calculated by Eqs. (8) & (9) respectively.

$$\ln \theta = \frac{1}{n} \sum_{i=1}^n \ln \hat{S}_{a1,i} \quad (8)$$

$$\beta = \sqrt{\frac{1}{n-1} \sum_{i=1}^n (\ln(\hat{S}_{a1,i}/\theta))^2} \quad (9)$$

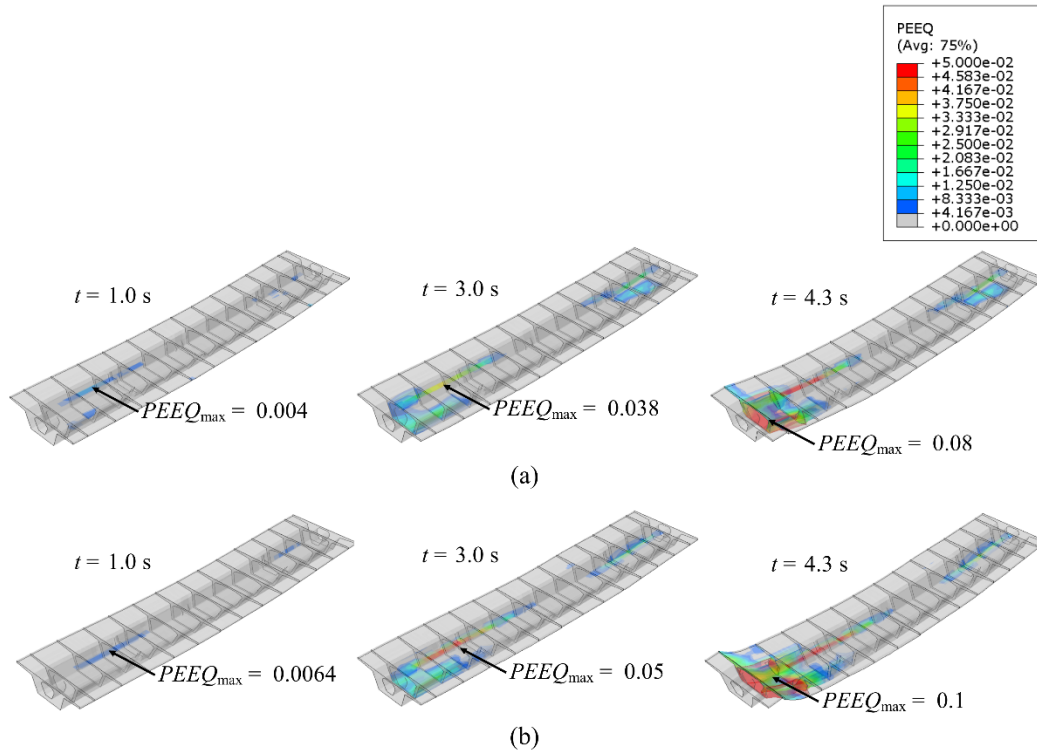


Fig. 5 – Damage evolution in the PT-PCSBs under the KOTA excitations: (a) model with $0.8P_e$ ($PGA_h = 2.4$ g; $S_{a1}^T = 3.97$ g & $S_{a1}^L = 2.88$ g) ; (b) model with P_e ($PGA_h = 2.8$ g; $S_{a1}^T = 4.63$ g & $S_{a1}^L = 3.37$ g).

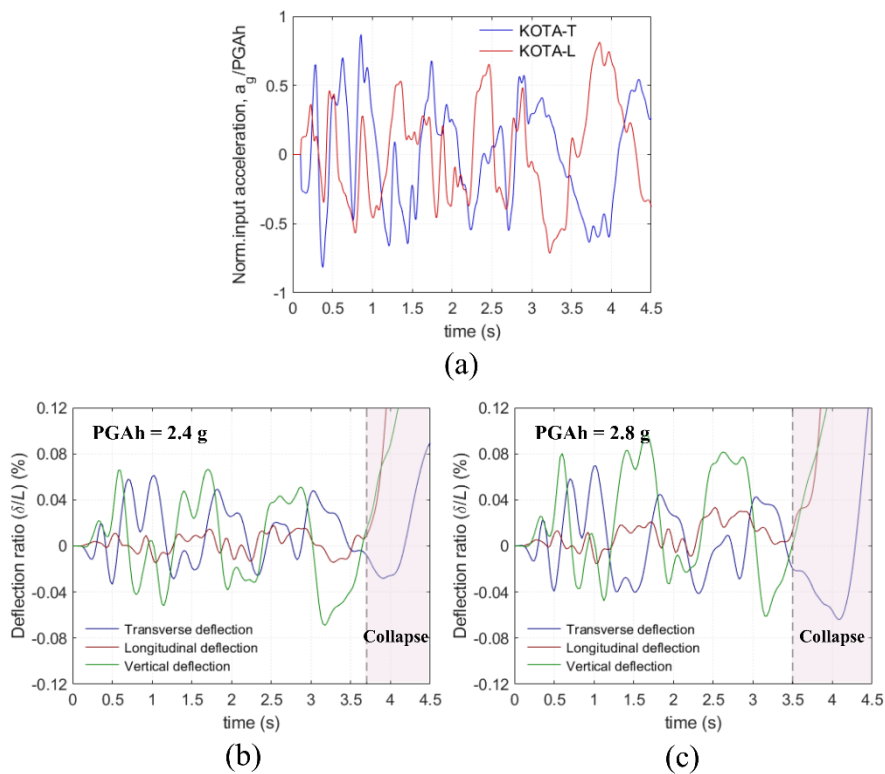


Fig. 6 – (a) Input acceleration time history of KOTA normalised w.r.t PGA_h ; displacement response time histories of (b) model with $0.8P_e$ at $PGA_h = 2.4$ g and (c) model with P_e at $PGA_h = 2.8$ g.

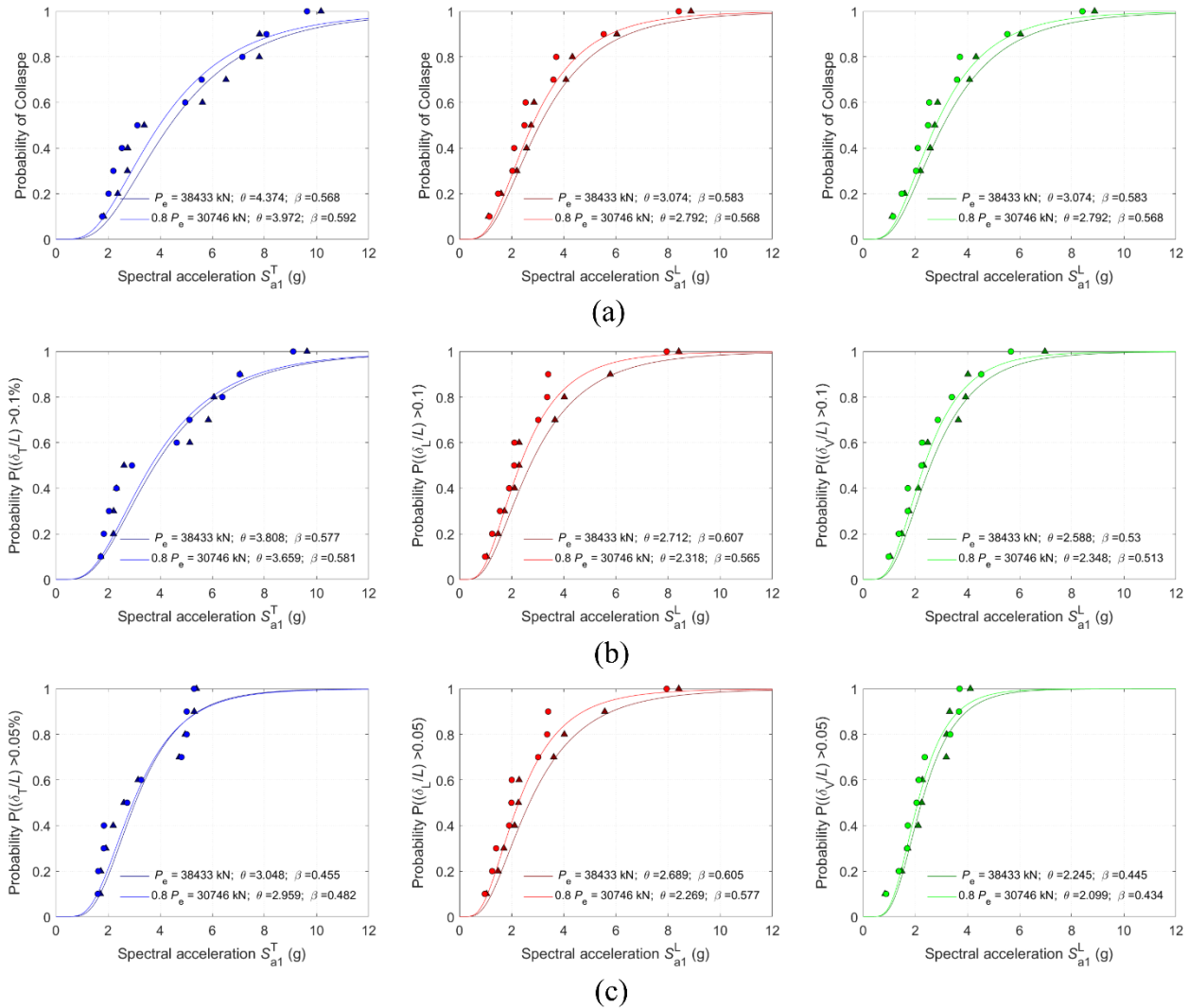


Fig. 7 – Fragility curves for the (a) collapse state, and deflection limit states of (b) $(\Delta/L)_{\text{limit}}^1 = 0.1\%$ and (c) $(\Delta/L)_{\text{limit}}^2 = 0.05\%$.

Based on the IDA performed above, the fragility functions associated with the transverse, vertical, and longitudinal deflections are constructed for PT-PCSB with $P_e = 38433$ kN and PT-PCSB with $0.8P_e = 30746$ kN as shown in Figs. 7 (a), (b) & (c) respectively. While the 20% reduction in the prestress does not significantly affect the exceedance probability of the deflection limit state at 0.05% for the transverse and vertical deflections, the exceedance probabilities of collapse and the deflection limit state at 0.1% increase by about 5% at a specific spectral acceleration between 2 g to 8 g. Nevertheless, the longitudinal responses show the opposite trend that the loss of prestress increases the exceedance probability of a small deflection limit (10% increase for 0.05% limit around $S_{a1}^L = 4$ g) more than the collapse probability (5% increase).

The average attainable spectral accelerations at the first mode at the collapse limit reduced by about 10% from $\theta = [\bar{S}_{a1}^T = 4.37, \bar{S}_{a1}^L = 3.07]$ g for PT-PCSB with P_e to $\theta = [\bar{S}_{a1}^T = 3.97, \bar{S}_{a1}^L = 2.79]$ g for PT-PCSB with $0.8P_e$. The change in the variations of the attainable spectral accelerations for different limit states is not strongly correlated with the prestress loss. As also demonstrated by the response time histories under KOTA excitations (Fig. 6), the vertical vibrations are more sensitive to the prestress changes and the structural capacity as indicated by PGAh reduced by 14.3% from 2.8 g to 2.4 g due to the 20% prestress loss.



4. Conclusions

Unexpected prestress loss due to poor maintenance and inaccurate estimation at design can significantly alter the structural performances of post-tensioned precast concrete segmental bridges (PT-PCSBs) with unbonded tendons. In this regard, the effects of prestress loss on the structural capacity and the exceedance probabilities of collapse and different deflection limits were investigated using Incremental Dynamic Analysis and Fragility Analysis with detailed discrete finite element (DFEM) models. Based on the analysis results, the following conclusions are drawn:

1. A 20% loss of prestress can lead to 10% to as much as 14% reduction in the structural load-carrying capacity and 5% increase in the collapse probability.
2. Significant inelastic deformation or even collapse of the PT-PCSBs occurred before the transverse deflection ratio reached 0.1% L .
3. The longitudinal and vertical vibrations are strongly coupled that significant vertical vibrations are induced by the longitudinal excitations without the introduction of any vertical excitations.
4. Yielding or the significant change of stiffness occurred at a transverse deflection ratio around 0.05% where inelastic deformation begins to develop near the end segments.
5. Collapse of the PT-PCSBs under the self-weight follows the significant damage developed near the end segments.
6. While the exceedance probabilities of small deflection limits for the transverse and vertical responses are not sensitive to the prestress loss, the longitudinal responses at low GM intensities are significantly affected.
7. For the longitudinal responses, the exceedance probability of a small deflection limit (0.05% L) increases by 10% due to 20% prestress loss.

5. Acknowledgments

The support of the Ministry of Science and Technology (MOST), R.O.C. under Grand Numbers 107-2636-E-009-002- and 108-2636-E-009-005- are gratefully acknowledged.

6. References

- [1] Hurst MK (2017): *Prestressed Concrete Design*. Taylor & Francis Group, New York, 2nd edition.
- [2] Ou YC, Wang PH, Tsai MS, Chang KC, Lee GC (2010): Large-scale experimental study of precast segmental unbonded posttensioned concrete bridge columns for seismic regions. *Journal of Structural Engineering*, **136** (3), 255–264.
- [3] ACI-ASCE Committee 423 (2016): *Guide to Estimating Prestress Loss*. Farmington Hills, MI: ACI.
- [4] Weiher H, Zilch K (2006): Condition of post-tensioned concrete bridges - assessment of the German stock by a spot survey of damages. *Proceedings of the First International Conference on Advances in Bridge Engineering*, London, UK.
- [5] Dawood H, Elgawady M, Hewes J (2012): Behavior of segmental precast posttensioned bridge piers under lateral loads. *Journal of Bridge Engineering*, **17** (5), 735–746.
- [6] Yuen TYP, Deb T, Zhang H, Liu Y (2019): A fracture energy based damage-plasticity interfacial constitutive law for discrete finite element modelling of masonry structures. *Computers & Structures*, **220**, 92–113.
- [7] Takebayashi T, Deeprasertwong K, Leung YW (1994): A full-scale destructive test of a precast segmental box girder bridge with dry joints and external tendons. *Proceedings of the Institution of Civil Engineers - Structures and Buildings*, **104** (3), 297–315.
- [8] AASHTO (1989): *Guide Specifications for Design and Construction of Segmental Bridges*. The American Association of State Highway and Transportation Officials, Washington DC.



- [9] ABAQUS Inc (2014): *Abaqus Analysis User's Guide*.
- [10] CEN (2004): *Eurocode 2: Design of Concrete Structures. Part 1: General Rules and Rules for Buildings* (EN 1992-1-1:2004). European Committee for Standardization, Brussels.
- [11] Lubliner J, Oliver J, Oller S, Oñate E (1989): A plastic-damage model for concrete. *International Journal of Solids and Structures*, **25** (3), 299–326.
- [12] Krätzig WB, Pölling R (2004): An elasto-plastic damage model for reinforced concrete with minimum number of material parameters. *Computers & Structures*, **82** (15–16), 1201–1215.
- [13] CEB-FIP (2012): *Model Code 2010 - Final version*, Vol. 1. vol. 1. fédération internationale du béton, Bulletin 66, Lausanne, Switzerland.
- [14] CEN (2004): *Eurocode 8: Design Of Structures for Earthquake Resistance. Part 1: General Rules, Seismic Actions and Rules for Buildings* (EN 1998-1:2004). European Committee for Standardization, Brussels.
- [15] Afshari K, Stewart JP (2016): Physically parameterized prediction equations for significant duration in active crustal regions. *Earthquake Spectra* 2016, **32** (4), 2057–2081.
- [16] Vamvatsikos D, Cornell CA (2002): Incremental dynamic analysis. *Earthquake Engineering & Structural Dynamics*, **31** (3), 491–514.
- [17] AASHTO (2010): *AASHTO LRFD Bridge Design Specifications*. American Association of State Highway and Transportation Officials, Washington, DC, 5th edition.
- [18] Baker JW (2015): Efficient analytical fragility function fitting using dynamic structural analysis. *Earthquake Spectra*, **31** (1), 579–599.